Low-Field Magnetic Separation of Monodisperse Fe$_3$O$_4$ Nanocrystals

Cafer T. Yavuz,[1] J. T. Mayo,[1] William W. Yu,[1] Arjun Prakash,[2] Joshua C. Falkner,[1] Sujin Yean,[3] Lili Cong,[3] Heather J. Shipley,[3] Amy Kan,[3] Mason Tomson,[3] Douglas Natelson,[4] Vicki L. Colvin[1]*

Magnetic separations at very low magnetic field gradients (<100 tesla per meter) can now be applied to diverse problems, such as point-of-use water purification and the simultaneous separation of complex mixtures. High–surface area and monodisperse magnetite (Fe$_3$O$_4$) nanocrystals (NCs) were shown to respond to low fields in a size-dependent fashion. The particles apparently do not act independently in the separation but rather reversibly aggregate through the resulting high-field gradients present at their surfaces. Using the high specific surface area of Fe$_3$O$_4$ NCs that were 12 nanometers in diameter, we reduced the mass of waste associated with arsenic removal from water by orders of magnitude. Additionally, the size dependence of magnetic separation permitted mixtures of 4- and 12-nanometer–sized Fe$_3$O$_4$ NCs to be separated by the application of different magnetic fields.

The removal of particles from solution with the use of magnetic fields is more selective and efficient (and often much faster) than centrifugation or filtration (1–3) and, as a result, magnetic separations are used in areas as diverse as biotechnology and ore refinement (4–7). Central to the process is the generation of magnetic forces on particles large enough to overcome opposing forces, such as Brownian motion, viscous drag, and sedimentation (8). In biotechnology, magnetic separators use relatively low field gradients in a batch mode to concentrate surface-engineered magnetic beads from a suspension (9, 10). In manufacturing, magnetic materials are typically recovered from waste streams under flow conditions with high-gradient magnetic separators (HGMS) that use larger fields (up to 2 T) and columns filled with ferromagnetic materials (11, 12).

Decreasing the particle sizes used in magnetic separations from micrometers to nanometers would increase the available sorptive areas by 100 to 1000 times. Such material optimization, however, is not generally practical, because the magnetic force acting on a particle in a field gradient is proportional to the particle volume. If the particles are too small, their magnetic tractive forces in a field gradient will not be large enough to overcome Brownian motion, and no separation will occur (13–15). For iron oxide, extrapolations from the behavior of

the bulk material suggest that the critical size for separation is ~50 nm for the case of an isolated (nonaggregated) particle (13). This treatment assumes very large applied fields and the latest designs for extremely high-gradient separators, both features that make magnetic separations prohibitively expensive in many settings (3, 16). For simpler and less costly low-gradient separators, the critical size for capture in magnetic gradients increases substantially.

Extrapolations from bulk properties to nanoscale materials are frequently problematic, and a more comprehensive analysis of nanoscale magnetic behavior suggests that nanocrystals (NCs) could offer substantial opportunities for low-field magnetic separations. Below 50 nm in diameter, nanoscale magnets exhibit a complex range of size-dependent behaviors, including a transition below ~40 nm in size to single-domain character (17, 18), magnetic susceptibilities greater than that of the bulk material (19, 20), and the emergence of superparamagnetic behavior (17). Such systems could experience larger than expected magnetic forces from bulk behavior due to larger moments. Hutten and co-workers have suggested the advantages of higher-susceptibility materials, such as FeCo, in which an increased magnetic moment could in principle enable high-gradient separations with isolated NCs (7, 21). Additionally, in external fields, the large surface gradients present at the surfaces of single-domain materials could induce transient aggregation, effectively forming larger and more magnetically responsive particles. Laibinis and co-workers suggested nanoparticle aggregation, even before field application, to explain their observation of the magnetic capture of polydisperse NCs in a high-gradient separation (>1000 T/m) using fields of 1 to 2 T (16, 22).

We show that magnetite (Fe$_3$O$_4$) particles of a critical size (20 nm) can be removed from solution at very low field gradients (<100 T/m)

and present evidence that aggregation, caused by the high field gradients at the nanoparticle surfaces, helps drive this process. To determine whether a critical size exists for this low-field separation, we have prepared Fe$_3$O$_4$ NCs that are highly monodisperse in size and nonaggregated in both aqueous and organic solutions (figs. S1 to S5) (23–25). Having previously established that the surfaces of nanocrystalline Fe$_3$O$_4$ particles are useful in the context of As removal from solution, we will use this problem as an example of a high-throughput separation (26).

Nanocrystalline Fe$_3$O$_4$ particles could be removed from solution with a low-gradient separator (23 T/m) like those applied to the recovery of micrometer-sized beads in protein purification. The initial rust-colored solution contained 16-nm-diameter Fe$_3$O$_4$ NCs homogeneously dispersed in water (Fig. 1A). Once placed in the separator, the solution became clear within minutes, and a deposit of particles formed at the back of the vial, where the field gradient was the largest (Fig. 1B). After removal from the separator, the solution could be restored to its initial state with a vigorous shake. Similar behavior was observed for all NCs larger than ~10 nm in diameter, but the time for complete separation varied with solution concentration and NC size.

The removal of NCs cannot be explained with a simple model of noninteracting particles. If we assume that the iron oxide particles act independently, we may calculate a size threshold below which NCs will not be removed. For a field gradient ∇B of 23 T/m, the largest magnetic force F_{mag} that can be applied to a single particle
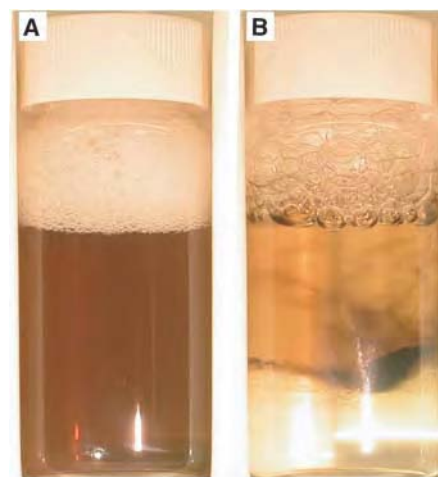

Fig. 1. Magnetic batch separation of 16-nm water-soluble Fe$_3$O$_4$ NCs with a conventional separator (Dexter Magnetic LifeSep 50SX). The field gradient at full field was 23.3 T/m. (**A**) Appearance of the solution immediately after placement in the separator. (**B**) After several minutes, the initially homogeneous solution became heterogeneous, and a black deposit formed on the back wall where the field gradient was the highest.

[1]Department of Chemistry, Rice University, 6100 Main Street, Houston, TX 77005, USA. [2]Department of Chemical and Biomolecular Engineering, Rice University, 6100 Main Street, Houston, TX 77005, USA. [3]Department of Civil and Environmental Engineering, Rice University, 6100 Main Street, Houston, TX 77005, USA. [4]Department of Physics and Astronomy, Rice University, 6100 Main Street, Houston, TX 77005, USA.

*To whom correspondence should be addressed. E-mail: colvin@rice.edu

of diameter d is $F_{mag} = \frac{4\pi}{3}\left(\frac{d}{2}\right)^3 M_{sat}\nabla B$, where M_{sat} is the saturation magnetization of the material. In order for these particles to separate effectively, this force must exceed the typical Brownian force $F_B \sim \frac{k_B T}{d}$, where T is temperature and k_B is Boltzmann's constant. For Fe_3O_4, with $M_{sat} = 4.69 \times 10^5$ A/m, at 300 K, this implies that independent particles smaller than ~160 nm in diameter will not separate in the low field gradients that were used. The previous analysis ignores the fact that the application of an external field will generate extremely large field gradients (up to $\mu_0 M_{sat}/d$, where μ_0 is the permeability of free space) at the surfaces of single-domain particles. Even in the absence of a field, magnetic NCs may interact as a result of magnetic dipole-dipole interactions [27]. In the presence of a field, these surface gradients could generate chains or aggregates of NCs. Once the field is removed, surface gradients would disappear and particle interactions would diminish. This reversible aggregation provides the advantages of a high–surface area nanocrystalline sorbent, without sacrificing the ability to separate the materials in a reasonable field gradient.

We characterized the size dependence of the NC separation process using an HGMS. Unlike the simple batch separator used in Fig. 1, this system uses an electromagnet to generate external fields of variable strength around a column packed with ferromagnetic wire. Exact measures of the field gradients in such a system are challenging to obtain, but most treatments predict that the gradient and the applied external field are proportional and that, at fields in excess of 1 T, gradients of 10^4 T/m are possible [28, 29]. Fe_3O_4 NCs of varying sizes were gravity-fed into the 22.3-cm-long column at various field strengths, and the effluent was collected and analyzed for iron content by means of inductively coupled plasma atomic emission spectroscopy (ICP-AES). From such experiments, we calculated the fraction of material retained in the column at increasing magnetic field strengths and compared these retention efficiencies between samples (Fig. 2A).

The size dependence of the retention of NCs in the magnetized column is shown in Fig. 2A. The amount of material retained in the column increased as the external field strength increased. For example, nearly 100% of the 12-nm-diameter NCs were retained in the column at applied fields of only 0.2 T, well below the saturation field for stainless steel. This same field, however, could not capture NCs less than 8.0 nm in diameter. Figure 2B shows that for all particles, as the particle size became smaller, more field was required to ensure their complete separation. This result parallels the observation (fig. S1C) that, at low field strengths, small NCs are not fully aligned. Without complete alignment, the magnetic moments of NCs would be quite small and would not generate enough tractive force with external field gradients [19, 30].

Fig. 2. (**A**) Size-dependent magnetic separation of 4.0-, 6.0-, 9.1-, 12-, and 20-nm Fe_3O_4 NCs in a column separator. A hexane dispersion of NCs was passed through a stainless steel column packed with 15 g of stainless steel wool; solutions were introduced at 20 ml/min by way of a gravity feed. The column was held in an S. G. Frantz canister separator (tunable field 0 to 1.6 T). After each data point was taken, the packing was removed, and the column was washed thoroughly, dried in an oven (at 60°C), and packed with clean, unused, stainless steel wool. Fractions collected at each data point were digested in concentrated HNO_3 and diluted to 5.5% HNO_3 before iron content analysis by means of ICP-AES. The percent retention was calculated by dividing the atomic iron concentration in a solution by the concentration found for the starting (unseparated) suspension. The curves presented are complex polynomials meant to guide the display and are not reflective of any physical model. These data illustrate that the smaller the NC, the greater the magnetic field required to retain the NC in the column. The 20-nm-diameter particles permanently affixed to the column after removal of the field. (**B**) The absolute field required to retain 100% of the NCs loaded to the stainless steel column (black points and curve) versus the diameter of Fe_3O_4 NCs. Also shown (blue points and curve) are the fractions of material that were unrecoverable after washing the column. The shaded area represents the optimal size for magnetic separations. For 4.0- and 6.0-nm particles, materials that were not completely retained, the absolute field for complete retention was estimated from their low-field behavior.
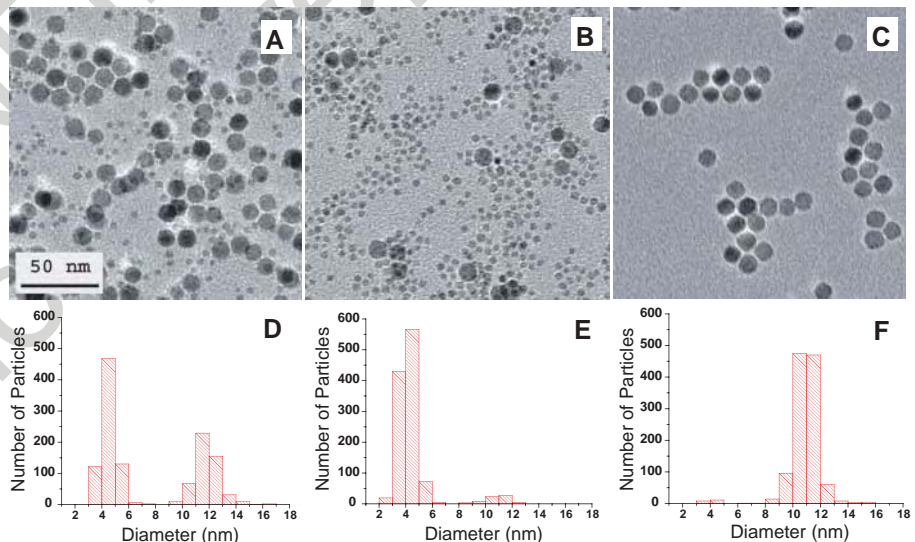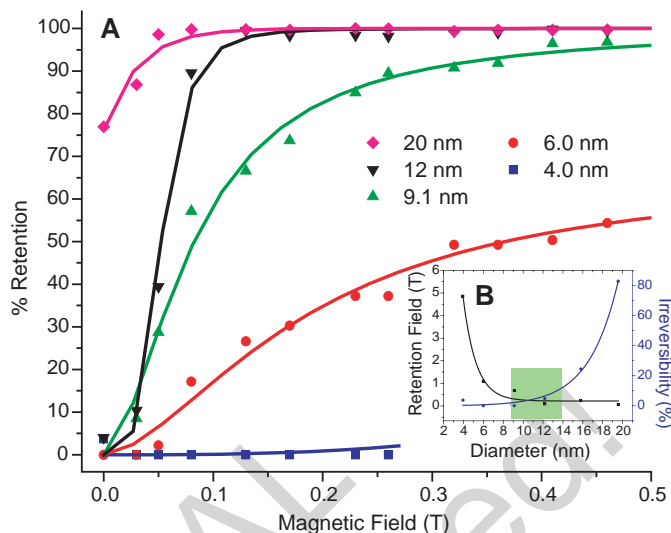

Fig. 3. Multiplexed separation of NC mixtures. 4.0- and 12-nm Fe_3O_4 NC solutions (both in hexane dispersions) were mixed in a 1:3 ratio (volume/volume) to achieve a particle mixture that contained roughly the same concentration of each size. With the use of an S. G. Frantz canister separator (Model L1-CN), the mixture separated into two size fractions, depending on the field. (**A**) Transmission electron microscopic (TEM) micrograph of the initial bimodal mixture. Scale bar in (A) is for (A) to (C). (**B**) TEM micrograph of the high-field (0.3 T) fraction. 94.4% of the 4.0-nm particles and <3% of the 12-nm particles were recovered. (**C**) TEM micrograph of low-field (0.03 T) fraction. 98.3% of larger (12 nm) NCs were collected. (**D** to **F**) Size-distribution histograms for particles counted in (A) to (C), respectively. In (A), two different populations were observed. In (B), the smaller size range was apparent as observed in the TEM micrograph. In (C), the larger sizes were successfully recovered after separation. For all size histograms, >1000 particles were counted in multiple images and measured automatically with the use of the software package ImagePro.

The size of NCs can also influence their recovery after magnetic capture. As seen in Fig. 2A, at zero external field (after the columns were magnetized), NCs that were 20 nm in diameter could not be removed from the column matrix even after repeated washes. This irreversible interaction is analogous to the fouling of a physical filter and would limit the use of larger magnetic sorbents in a commercial setting. Smaller NCs, however, did not show such behavior and could be concentrated and reused quite easily (Fig. 2B). This observation stems from the fact that iron oxide NCs less than ~16 nm in diameter behave as superparamagnets (17, 30–33). In this limit, NCs have no net magnetization (fig. S1E) and thus experience no interactions with the very small stray fields present in the ferromagnetic column matrix (34). This result is consistent with observations

of commercial magnetic beads, which found that, even in micrometer-sized systems, there was much value in the use of magnetic materials that were superparamagnetic (35, 36). The data shown here reveal that superparamagnetism is only one of several properties that should be considered in material design. Indeed, if NCs are too small, then magnetic separations require very large critical field strengths to affect any capture of particles (Fig. 2B). For optimal NC magnetic separations at low fields, one should use the largest NCs that still show superparamagnetic properties.

The size dependence of NC capture (Fig. 2A) now makes it possible to develop magnetic separation processes that can, in one process, remove several different types of materials. Such capability is particularly important in biotechnology, in which the simultaneous treatment of mixtures requires more sophisticated multiplexed separations (37). Figure 3 demonstrates the principle for magnetic separations, in which different field strengths recovered different populations of bimodally distributed iron oxide NCs. Initially, the sample consisted of two monodisperse fractions of NCs, intentionally combined to create a test solution (Fig. 3A); at low applied fields (0.3 T), the effluent from the column contained >90% of the smaller particles, and the larger particles were retained in solution (Fig. 3B). After the field was turned off, a column wash recovered the larger particles (Fig. 3C). With the use of monodisperse iron oxide NCs, it is thus possible to use

magnetic separations in a multiplexed mode and recover different components of a mixture in one treatment.

Because NCs can be removed from batch solutions with the use of permanent handheld magnets, we explored whether these NCs could act as effective magnetic sorbents for the removal of As from water. Arsenic is a good model contaminant for these materials, because its interaction with iron oxides is strong and irreversible, even on nanoscale particles (26, 38). Its practical and effective removal from groundwater remains an important and intractable problem in water treatment (39, 40). Conventional HGMSs operating at ≥1T are already used in water treatment processes, primarily to induce the aggregation of intrinsically magnetic waste products that are not easily amenable to other methods of coagulation (12, 26, 41, 42).

Both As(III) and As(V) exhibit strong adsorption onto iron oxide nanocrystalline surfaces; as the concentration of As increased in the standard solution, the amount of As bound to NCs increased as well, until the capacity of the material was reached (Fig. 4). The interactions between iron oxide and As are also irreversible, so Fe_3O_4 NCs that have bound As should not release the material back into the environment during storage and further treatment. These data show clearly that as the size of sorbent NCs decreases, sorption capacities increase substantially because of the increased surface areas in the samples.

Once As was sorbed onto NC surfaces, magnetic separations provided a way to remove the materials from solution. The As concentrations in test solutions before and after the removal of particles by means of a column magnetic separator (Table 1 and table S1) showed that As(III) and As(V) could be reduced to well below the current U.S. standards for drinking water (43). Also, because the test NCs are very small (12 nm), their very high specific surface areas provide extremely concentrated waste materials. For example, 300-nm-sized iron oxide particles have a sorption capacity of only 0.002% by weight, and thus, treating 50 liters of solution with 500 μg of As per liter generates 1.4 kg of waste; in contrast, for an equivalent treatment, only 15 g of 12-nm-sized iron oxide sorbent is required.
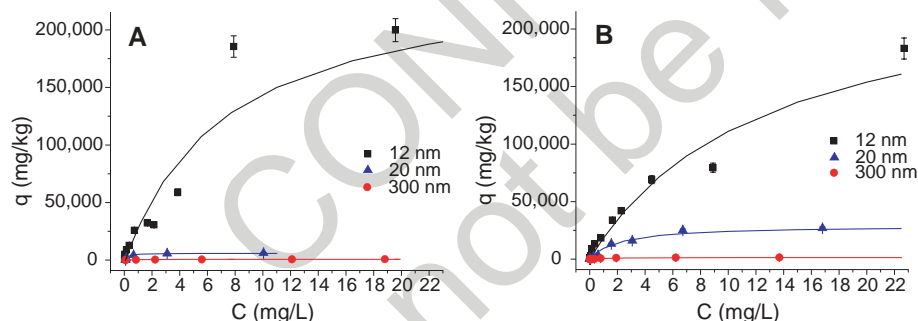
Table 1. A comparison of As removal efficiency, assuming a treatment of 2 liters of As solution (500 μg/liter) with 1 g of Fe_3O_4.

Particle size (nm)	As(V) or As(III)	Residual As concentration (μg/liter)	% removal
12	As(III)	3.9	99.2
20	As(III)	45.3	90.9
300	As(III)	375.7	24.9
12	As(V)	7.8	98.4
20	As(V)	17.3	96.5
300	As(V)	354.1	29.2

Fig. 4. Arsenic adsorption studies with nanocrystalline (12 nm) and commercially available (20 and 300 nm) Fe_3O_4. The smaller (12 nm) Fe_3O_4 particles were made water-soluble by means of a surfactant; for this, the NC was sonicated with an aqueous dispersion of a secondary surfactant, Igepal CO 630, and then purified by sedimentation [50,000 revolutions per minute (141,000g)]. Arsenic adsorption experiments were performed with 25 μg/liter to 25 mg/liter of As(III) and As(V) solutions, prepared in an electrolyte solution containing 0.01 M NaCl, 0.01 M tris(hydroxymethylamino)methane buffer, and 0.01 M NaN_3 at pH 8. All experiments were performed in batches with 10 and 100 mg of Fe_3O_4 per liter of solution for the 12- and 20-nm particles, respectively, and 2.5 g of Fe_3O_4 per liter of solution for the 300-nm particles. Equilibrium time was 24 hours, with constant tumbling. The solution was separated from Fe_3O_4 by a magnetic field column separator [S. G. Frantz canister separator (Model L1-CN)]. After the effluent was collected, the magnet was turned off, and 40 ml of deionized water was passed through the separator to elute Fe_3O_4. All effluents were acidified with trace-metal grade HNO_3 to contain 1% HNO_3 in solution. Arsenic concentration was measured with inductively coupled plasma mass spectrometry (ICP-MS). The nanoscale Fe_3O_4 was acid-digested, and the Fe and As concentrations in the digest were measured by ICP-AES and ICP-MS, respectively. (**A**) As(V) adsorption to magnetites of different size; (**B**) As(III) adsorption. C, arsenic concentration in solution; q, adsorption capacity. Errors bars in (A) and (B) indicate 5% error in the measurement of arsenic.

References and Notes
1. S. C. Chang et al., J. Ind. Microbiol. Biotechnol. **32**, 629 (2005).
2. J. J. Hubbuch, D. B. Matthiesen, T. J. Hobley, O. R. T. Thomas, Bioseparation **10**, 99 (2001).
3. B. L. Hirschbein, D. W. Brown, G. M. Whitesides, Chemtech **12**, 172 (1982).
4. C. G. Gunther, Electro-Magnetic Ore Separation (Hill, New York, 1909).
5. R. Gerber, R. R. Birss, High Gradient Magnetic Separation (Research Studies, New York, 1983).
6. J. Oberteuffer, IEEE Trans. Magn. **10**, 223 (1974).
7. G. Reiss, A. Hutten, Nat. Mater. **4**, 725 (2005).
8. J. H. P. Watson, J. Appl. Phys. **44**, 4209 (1973).
9. M. Lewin et al., Nat. Biotechnol. **18**, 410 (2000).

10. J. M. Nam, C. S. Thaxton, C. A. Mirkin, *Science* **301**, 1884 (2003).
11. C. H. Setchell, *J. Chem. Technol. Biotechnol. B Biotechnol.* **35**, 175 (1985).
12. C. Delatour, *IEEE Trans. Magn.* **9**, 314 (1973).
13. D. Fletcher, *IEEE Trans. Magn.* **27**, 3655 (1991).
14. D. R. Kelland, *IEEE Trans. Magn.* **34**, 2123 (1998).
15. G. B. Cotten, H. B. Eldredge, *Sep. Sci. Technol.* **37**, 3755 (2002).
16. G. D. Moeser, K. A. Roach, W. H. Green, T. A. Hatton, P. E. Laibinis, *Am. Inst. Chem. Eng. J.* **50**, 2835 (2004).
17. H. U. Worm, *Geophys. J. Int.* **133**, 201 (1998).
18. R. F. Butler, *Paleomagnetism: Magnetic Domains to Geologic Terranes* (Blackwell Scientific, Boston, 1992).
19. D. Horak, F. Lednicky, E. Petrovsky, A. Kapicka, *Macromol. Mater. Eng.* **289**, 341 (2004).
20. G. F. Goya, T. S. Berquo, F. C. Fonseca, M. P. Morales, *J. Appl. Phys.* **94**, 3520 (2003).
21. A. Hutten *et al.*, *J. Biotechnol.* **112**, 47 (2004).
22. A. Ditsch, S. Lindenmann, P. E. Laibinis, D. I. C. Wang, T. A. Hatton, *Ind. Eng. Chem. Res.* **44**, 6824 (2005).
23. See the supporting material on *Science* Online for supplementary data.
24. W. W. Yu, J. C. Falkner, C. T. Yavuz, V. L. Colvin, *Chem. Commun.* **2004**, 2306 (2004).
25. S. H. Sun, H. Zeng, *J. Am. Chem. Soc.* **124**, 8204 (2002).
26. S. Yean *et al.*, *J. Mater. Res.* **20**, 3255 (2005).
27. K. Butter, P. H. H. Bomans, P. M. Frederik, G. J. Vroege, A. P. Philipse, *Nat. Mater.* **2**, 88 (2003).
28. M. R. Parker, *Phys. Technol.* **12**, 263 (1981).
29. G. Iacob, A. Ciochina, O. Bredetean, *Eur. Cell. Mater.* **3**, 167 (2002).
30. A. R. Muxworthy, *Geophys. J. Int.* **144**, 441 (2001).
31. S. Bucak, D. A. Jones, P. E. Laibinis, T. A. Hatton, *Biotechnol. Prog.* **19**, 477 (2003).
32. R. F. Butler, S. K. Banerjee, *J. Geophys. Res.* **80**, 4049 (1975).
33. J. A. Dearing *et al.*, *Geophys. J. Int.* **124**, 228 (1996).
34. R. D. Ambashta, P. K. Wattal, S. Singh, D. Bahadur, *J. Magn. Magn. Mater.* **267**, 335 (2003).
35. B. I. Haukanes, C. Kvam, *Nat. Biotechnol.* **11**, 60 (1993).
36. G. P. Hatch, R. E. Stelter, *J. Magn. Magn. Mater.* **225**, 262 (2001).
37. G. Liu, J. Wang, J. Kim, M. R. Jan, G. E. Collins, *Anal. Chem.* **76**, 7126 (2004).
38. S. R. Kanel, B. Manning, L. Charlet, H. Choi, *Environ. Sci. Technol.* **39**, 1291 (2005).
39. M. A. Hossain *et al.*, *Environ. Sci. Technol.* **39**, 4300 (2005).
40. L. G. Twidell, J. McCloskey, P. Miranda, M. Gale, in *Proceedings of the Global Symposium on Recycling, Waste Treatment and Clean Technology Conference*, San Sebastian, Spain, 5 to 9 September 1999 (The Minerals, Metals, and Materials Society, Warrendale, PA, 1999), pp. 1715–1726.
41. Y. Kakihara, T. Fukunishi, S. Takeda, S. Nishijima, A. Nakahira, *IEEE Trans. Appl. Supercond.* **14**, 1565 (2004).
42. A. Chiba *et al.*, *IEEE Trans. Appl. Supercond.* **12**, 952 (2002).
43. U.S. Environmental Protection Agency Arsenic Rule, *Fed. Regist.* **66**, 6976 (22 January 2001) [40 Code of Federal Regulations] (www.epa.gov/safewater/arsenic/regulations.html).
44. We thank NSF for its support of the Center for Biological and Environmental Nanotechnology (EEC-0647452). We also acknowledge with gratitude the Office of Naval Research (N00014-04-1-0003), and the U.S. Environmental Protection Agency Star Program (RD-83253601-0) for funding. C.T.Y. thanks the Robert A. Welch Foundation (C-1349) for a graduate fellowship. D. M. Mittleman provided invaluable help in developing this manuscript. Finally, the authors appreciate the efforts of J. Jones and W. Guo, who provided support for the supporting figures included on *Science* Online.

Localized Temporal Change of the Earth's Inner Core Boundary

Lianxing Wen

Compressional waves of an earthquake doublet (two events occurring in the South Sandwich Islands on 1 December 1993 and 6 September 2003), recorded at three seismic stations in Russia and Kyrgyzstan and reflected off Earth's inner core boundary, arrived at least from 39 to 70 milliseconds earlier in the 2003 event than in the 1993 event. Such changes indicate that Earth's inner core radius enlarged locally beneath middle Africa by 0.98 to 1.75 kilometers between the times of these two events. Changes of the inner core radius may be explained by either a differential motion of the inner core, assuming that irregularities are present at the inner core boundary and fixed to the inner core, or a rapid growth of the inner core by this amount.

Earth's inner core grows from the solidification of the outer core (*1*). The growth of the inner core releases latent heat and dispels light elements, providing driving forces for the outer core convection (*2*) and power for generating the geodynamo (*3*, *4*). The inner core growth process is thought to be geologically slow (*5–10*) and geographically uniform because of the presumed extremely small variation in temperature in the outer core (*11*). Here, I used PKiKP [a compressional wave reflected off the inner core boundary (Fig. 1A)] waveforms of an earthquake waveform doublet discovered by Zhang *et al.* (*12*) to study temporal change of the inner core boundary.

Earthquake waveform doublets are earthquakes occurring at different times but in almost exactly the same location and generating similar waveforms (*12–18*). Because the relative travel time and waveform difference between the waveform doublets is sensitive only to the relative change of event location and/or the temporal change of seismic properties, it is powerful to use waveform doublets to study high-resolution relative locations of the earthquakes (*13–15*) and to detect temporal change of seismic properties (*12*, *16–18*). The similarities of the doublet waveforms also allow accurate travel time measurement to be made. Zhang *et al.* (*12*) reported the existence of 19 waveform doublets in the South Sandwich region over a period of 35 years and showed that the PKP(DF) (PKIKP) phases [a compressional wave propagating through the inner core (Fig. 1A)] are in misalignment to each other between the doublets. Their study provided compelling evidence for the reported temporal changes in PKIKP travel time (*19–21*). They further proposed that the observed temporal changes can be explained by an inner core differential motion over a lateral velocity gradient in the inner core (*20*).

I used the best doublet reported in Zhang *et al.* (*12*) (table S1). The doublet consists of two events occurring on 1 December 1993 (event 93) and 6 September 2003 (event 03). I used the observed difference in absolute arrival time of various seismic phases that are not associated with the inner core (non-IC phases) between the doublet to determine the relative location and origin time of the two events. I used event 93 as the master event [i.e., fixed its origin time and location to those reported in the earthquake catalog (table S1)] and searched for the best-fitting relative location and origin time for event 03 that minimize the travel time residuals of the non-IC phases between the two events. I then studied the temporal changes of travel time and waveform of the PKiKP-PKIKP or PKiKP phases between the doublet based on the best-fitting relative hypocenter location and origin time of the two events. To do so, the PKiKP and PKiKP-PKIKP waveforms of the doublet were superimposed on the basis of the relative arrival times of these phases between the doublet, estimated using the best-fitting relative location and origin time of the two events. The PKiKP travel time residuals between the doublet are further calculated by subtracting the predicted relative arrival times of the seismic phases from the measured arrival time differences between the doublet. If the superimposed waveforms are in misalignment between the doublet, or if a travel time residual is larger than the relocation error bar, it would mean that the arrival times of the seismic phases between the doublet cannot be explained by the relative origin time and hypocenter location of the doublet, and these phases exhibit temporal change in time.

The detailed relocation analysis places the doublet within 0.37 km in horizontal space and 0.7 km in depth (*22*). The inferred best-fitting relative origin time and hypocenter location between the doublet yield, for the non-IC phases,

Department of Geosciences, State University of New York at Stony Brook, NY 11794, USA. E-mail: Lianxing.Wen@sunysb.edu